# Improved Outage Probability using Multi-IRS-Assisted MIMO Wireless Communications in Cellular Blockage Scenarios

Suresh Penchala, Shravan Kumar Bandari, and V.V. Mani

Abstract-Future wireless communication technologies must be upgraded to serve the upcoming seamless data-intensive applications and support a minimum information rate. To this end, an intelligent reflecting surface (IRS) technology was recently proposed as a viable solution to cover the uncovered regions with enhanced performance by means of a controlled wireless environment using multiple reflecting elements. In this paper, to elevate the end-user experience, we intend to improve the outage probability (OP) performance utilizing multiple IRS for multiple-input-multiple-output (MIMO) communication systems under a generalized  $\eta-\mu$  fading channel, which is suitable for non-line-of-sight (NLOS) scenarios. We derived a closed-form expression for OP and validated the same using a rigorous Monte-Carlo (MC) simulation setup under the considered system model. A comprehensive analysis of each system parameter impacting the likelihood that the communication channel supports the information rate has been detailed based on the number of IRSs, the number of reflecting elements, antenna count at transmitter and receiver, fading parameters, and the placement of IRSs. Results suggest that employing multiple IRSs reduces the outage scenarios in blockage zones, and further improvement can be observed with multiple antennas positioning the IRSs closer to either the transmitter or the receiver. Furthermore, we present an energy efficiency (EE) assessment for the multi-IRS system.

Index Terms—Intelligent reflecting surface, outage probability, multi-IRS, multi-antenna,  $\eta$ - $\mu$  fading channel.

## I. INTRODUCTION

The intelligent reflective surface (IRS) (a.k.a. reconfigurable intelligent surface) is emerging as a transformative technology with significant potential to influence the development of next-generation wireless communication systems, including 6G cellular networks [1]. In a nutshell, an IRS panel comprises multiple low-cost passive meta-material surface elements steered by a controller to guide the incident electromagnetic (EM) signals toward the intended direction by adjusting their reflecting angles to enhance the end-user experience by maximizing the received signal-to-noise ratio (SNR) [2]. The configuration thus established will now be able to control the uncontrollable wireless radio environment with ease, which has attracted significant attention from academia and industry [3], [4]. IRS technology tunes the beam (active/passive/jointly) to direct

Suresh Penchala and Shravan Kumar Bandari are with the Department of Electronics and Communication Engineering, National Institute of Technology Meghalaya, India (e-mail: penchalasuresh@gmail.com, shravnbandari@nitm.ac.in).

V.V. Mani is with the Department of Electronics and Communication Engineering, National Institute of Technology Warangal, India (e-mail: vvmani@nitw.ac.in).

DOI: 10.36244/ICJ.2025.3.5

electromagnetic waves toward a specified target [5]. This functionality enables IRS-assisted systems to mitigate deep-fading conditions by dynamically reconfiguring the wireless environment.

IRS technology is adaptable and suitable for various applications, covering indoor and outdoor wireless systems, 6G mobile networks, and satellite communications [6]. Various technological advancements, including multiple antenna systems [7], generalized frequency division multiplexing (GFDM) [8], [9], orthogonal time frequency space modulation (OTFS) [10], and network optimization [11], have been developed to enhance the performance of wireless communication. The utilization of the non-orthogonal multiple access (NOMA) scheme in the IRS application was examined in [12]. The authors in [13] employed an IRS to improve the performance of a dual-hop system that combines free-space optical and radio frequency (FSO-RF) technologies. Subsequently, the authors in [14] expanded their investigation on the IRS to include unmanned aerial vehicle (UAV) networks. Moreover, the concept of employing IRS-assisted transmission for efficient communication has been thoroughly examined in relation to co-operative relay [15], space shift keying [16], and backscatter communication technologies [17]. Recent studies have explored practical IRS deployment aspects such as indoor panel positioning and field trials for single and multi reflection architectures [18], as well as AI-driven control approaches like deep reinforcement learning applied to UAV-mounted IRS

On the other hand, wireless communication channels are subject to fading due to interactions like reflection, scattering, and diffraction as signals propagate. These effects cause fluctuations in signal strength and quality, which traditional models such as Rayleigh and Nakagami-m distributions only partially capture [20]. To address the limitations of these models, the  $\eta$ - $\mu$  fading channel was introduced as a more versatile framework [21]. It can describe a wide range of fading scenarios by accounting for diverse scattering environments and providing a better fit to experimental data. It is customary to analyze the performance of any new technology in an uncontrollable, random wireless fading environment. The deployment of IRS technology allows for improved control over channel conditions by intelligently positioning the IRS panel at desired locations. This helps mitigate channel randomness and enhances overall system performance in terms of bit/symbol error rates (BER/SER), Ergodic capacity, outage probability (OP), and energy efficiency (EE).

In [22], an IRS-assisted network in Nakagami-m fading was proposed, and closed-form expressions for the outage probability, average symbol error probability, and channel capacity were derived. Results suggest the superior performance of the IRS-aided communication system compared to the conventional one. Study in [23] examines the IRS technology in enhancing wireless communication under a Weibull fading channel. It highlights the improvement in spectral efficiency, outage probability, and SER through increased IRS elements and better phase accuracy. A dual IRS-assisted system with separate IRS placements near the source and destination, enabling communication without a direct link, was investigated in [24]. Closed-form OP and SER expressions are derived for Rician and Rayleigh fading, with results showing superior performance and energy efficiency compared to a single IRS setup. The OP of a single-input-single-output (SISO) wireless system using multiple IRS panels in  $\kappa$ - $\mu$  fading channels was investigated in [25]. Selecting the best IRS panel ensures optimal quality of service (QoS) for single-node communication. [26] investigates the OP and asymptotic sum rate in multi-IRS-assisted networks operating over Rayleigh fading channels. It was observed that the number of IRSs and the number of reflecting elements play an important role in the capacity scaling law of multiple RIS-aided networks. A system with multiple IRSs has been studied in [27] and analyzed under Rician fading conditions, focusing on the OP, which depends on the phase shifts of all IRSs. Studies demonstrate that utilizing multiple IRSs significantly enhances wireless communication in terms of coverage and service quality. The collaborative utilization of multiple IRSs significantly enhances the received signal power [28]. Furthermore, situating IRSs in diverse locations guarantees that signals can still access the receiver via alternative routes, even if certain paths encounter significant fading.

From these observations, it is crucial to highlight that the outage probability analysis of a multi-IRS-enabled MIMO communication system under  $\eta-\mu$  fading channels under the NLOS scenario between the transmitter (Tx) and the receiver (Rx) remains unexplored. Additionally, we adopt a more practical approach by modeling the fading behavior with an  $\eta-\mu$  channel, which more accurately represents real-world conditions. To address this gap, in this work, we intend to investigate the outage probability performance analysis of a multi-IRS-assisted communication system in a MIMO wireless fading channel environment. The key contributions of the proposed system model are summarized as follows:

- A versatile channel model for evaluating various IRS-assisted systems is highly significant. In this study, we adopt such a model for the Tx-IRSs and IRSs-Rx links, employing a generalized  $\eta$ - $\mu$  fading distribution combined with large-scale path loss, tailored for a multi-antenna MIMO communication system supported by multiple IRSs.
- Using the derived signal-to-noise ratio and the central limit theorem, we determined the mean and variance of the overall cascaded wireless channel links.

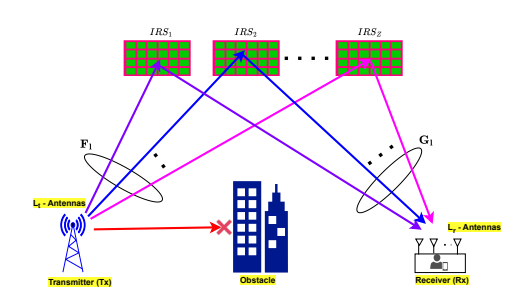


Fig. 1. Multi IRS aided MIMO wireless communication model

- A framework to find the probability that a user is in an outage scenario is also discussed through the obtained theoretical expression. For completeness, the energy efficiency comparing the multi-IRS system to the reference single-IRS system is also discussed.
- We demonstrated the optimal placement of the IRS, emphasizing its critical positioning near both the Tx and Rx for a fixed transmitted signal power.
- The theoretical expressions closely match the Monte Carlo (MC) simulations, validating the proposed multi-antenna, multi-IRS MIMO system in the  $\eta$ - $\mu$  channel. We also analyzed and highlighted the impact of key parameters on performance.

The structure of the paper is organized as follows: Section II describes the system model, Section III outlines the theoretical formulations for analyzing OP performance, Section IV outlines the energy efficiency, and Section V examines the results obtained through Monte Carlo simulations and analytical calculations. Finally, Section VI provides a discussion of the conclusions.

### II. SYSTEM MODEL

This paper explores the design of a MIMO wireless system with  $L_t$  antennas at the transmitter (Tx),  $L_r$  antennas at the receiver (Rx), and Z IRSs as shown in Fig. 1. The system operates under  $\eta$ - $\mu$  fading channels, and we derive a mathematical expression for the OP in the NLOS scenario. Notably, we consider the direct link between the Tx and Rx to be completely blocked due to tall buildings and is therefore excluded from the analysis. Combining the effects of all Z IRSs, the signal received at the Rx via Z independent paths can be expressed as [29],

$$y = \left[\sum_{l=1}^{Z} \sum_{i=1}^{N_l} \sum_{p=1}^{L_t} \sum_{q=1}^{L_r} g_{lip} r_{li} f_{liq}\right] x + n \tag{1}$$

The parameters of equation (1) along with their corresponding notations are listed in Table I.  $g_{lip}=d_{TI_l}^{-\frac{1}{2}}\delta_{lip}e^{-j\phi_{lip}}$  is the channel between the p-th Tx and the l-th IRS, where  $\delta_{lip}$  is the channel gain between the p-th Tx antenna and the i-th element of the l-th IRS,  $d_{TI_l}$  is the distance between the Tx and the l-th IRS, and  $\phi_{lip}$  is the phase of the Tx to the i-th element of the l-th IRS channel.  $f_{liq}=d_{I_lR}^{-\frac{5}{2}}\vartheta_{liq}e^{-j\psi_{liq}}$  is the channel between the l-th IRS and the q-th Rx, where  $\vartheta_{liq}$  is the channel gain

between the *i*-th IRS element and the *q*-th Rx antenna,  $d_{I_lR}$  is the distance between the *l*-th IRS and the Rx, and  $\psi_{liq}$  is the phase of the IRS-to-Rx channel.  $r_{li} = b_{li}e^{j\theta_{li}}$  is the reflection coefficient of the *i*-th element of the *l*-th IRS, where  $\theta_{li}$  is the phase shift applied by the *i*-th element of the *l*-th IRS. Additionally,  $\alpha$  represents the average path loss exponent. For simplicity, this study assumes the optimal phase shift (OPS) selection as  $\theta_{li} = \phi_{lip} + \psi_{liq}$  [30]. Assuming the optimal

TABLE I
PARAMETERS NOTATION SUMMARY

Symbol	Description
$L_t$	Number of transmit antennas
$L_r$	Number of receive antennas
Z	Number of IRS panels
$N_l$	Number of reflecting elements per IRS
x	Transmitted signal from Tx
У	Received signal at Rx
n	Additive white gaussian noise (AWGN)
$g_{lip}$	The channel between the $p$ -th Tx and the $l$ -th IRS
$f_{liq}$	The channel between the $l$ -th IRS and the $q$ -th Rx
$r_{li}$	IRS reflection coefficient
$\theta_{li}$	Phase shift applied by ith element of lth IRS
$d_{TIl}, d_{IlR}$	Tx-to-IRS and IRS-to-Rx distances
α	Path loss exponent
$\delta_{lip}$	Fading gain from Tx to IRS element
$\vartheta_{liq}$	Fading gain from IRS element to Rx
T	Effective cascaded channel gain
ζ	Normalization term for SNR
$\gamma$	Instantaneous received SNR
$\gamma_{ m th}$	Outage SNR threshold
$\Lambda_e, \Lambda_v^2$	Mean and variance of Υ
$\omega_m, \omega_v$	Mean and variance of $\eta$ - $\mu$ variables
η	Scattering parameter (η–μ model)
$\mu$	Clustering parameter ( $\eta$ – $\mu$ model)
$Q(\cdot)$	Gaussian Q-function
$Q_{1/2}(\cdot,\cdot)$	Generalized Marcum Q-function (order 1/2)

phase and perfect reflection ( $b_{li}=1$ ) at the IRS. In practical implementations, discrete phase shifting (DPS) is employed to restrict phase values to a finite set within the range  $[0,2\pi]$ , where the phase shift is given by  $\theta_{lip}=\frac{2\pi}{2^b}f$ , Here f can be  $0,1,\ldots,2^b-1$ , and b indicates how many digits are used to show each level [31]. As a result, the maximum received SNR at the Rx can be expressed as [32],

$$\gamma = \frac{\left(\sum_{l=1}^{Z} \sum_{i=1}^{N_{l}} \sum_{p=1}^{L_{t}} \sum_{q=1}^{L_{r}} d_{TI_{l}}^{-\frac{\alpha}{2}} \delta_{lip} d_{I_{l}R}^{-\frac{\alpha}{2}} \vartheta_{liq}\right)^{2} E_{x}}{N_{o}} 
= \frac{\Upsilon^{2} E_{x}}{\left(\sum_{l=1}^{Z} d_{TI_{l}}^{\alpha} d_{I_{l}R}^{\alpha}\right) N_{0}} = \Upsilon^{2} \zeta$$
(2)

where  $\Upsilon = \left(\sum_{l=1}^{Z}\sum_{i=1}^{N_l}\sum_{p=1}^{L_t}\sum_{q=1}^{L_r}\delta_{lip}\vartheta_{liq}\right),~\zeta = \frac{E_x}{\left(\sum_{l=1}^{Z}d_{Tl_l}^{\alpha}d_{l_lR}^{\alpha}\right)N_0}.$  When  $N_l$  is sufficiently large, the central limit theorem (CLT) suggests that  $\Upsilon$  is likely to follow a Gaussian distribution [33]. As a result,  $\gamma$  will follow a noncentral chi-squared (NCCS) distribution with one degree of freedom. Furthermore,  $\delta_{lip}$  and  $\vartheta_{liq}$  are assumed to be independent and identically distributed (IID)  $\eta-\mu$  random variables, characterized by the following probability density function (PDF) [9], [34],

TABLE II  $\eta$ - $\mu$  SPECIAL CASES

Description	η	$\mu$
Rayleigh	1	0.5
Nakagami-m	1	m/2
Nakagami-q (Hoyt)	$q^2$	0.5

$$f_{P}(\rho) = \frac{2\sqrt{\pi} (1+\eta)^{\mu+\frac{1}{2}} \rho^{2\mu}}{\sqrt{\eta} (1-\eta)^{\mu-\frac{1}{2}} \Gamma(\mu)}$$
$$\exp\left[-\frac{\mu (1+\eta)^{2} \rho^{2}}{2\eta}\right] I_{\mu-\frac{1}{2}} \left[\frac{\mu (1-\eta^{2}) \rho^{2}}{2\eta}\right]$$
(3)

where  $\Gamma(\cdot)$  refers to the Gamma function,  $I_n(\cdot)$  signifies the n-th modified Bessel function of the first kind,  $\eta$  represents the ratio of the non-centrality parameter to the scale parameter, primarily influencing the spread or variability of the fading envelope. The parameter  $\mu$  represents the shape parameter of the distribution, affecting the asymmetry of the fading envelope. The generalized  $\eta - \mu$  fading distribution is a versatile model capable of encompassing several other distributions, including Rayleigh, Nakagami-q, and Nakagami-m fading channels, as special cases shown in Table II. It is especially suitable for NLOS environments due to its capability to model the intricate characteristics of signal propagation, including non-uniform conditions influenced by scattering elements, reflective surfaces, and diffraction effects. The  $j^{th}$  moment of  $\eta - \mu$  distribution is given by [34],

$$E(P^{j}) = \frac{2^{(2\mu+j/2)}\Gamma(2\mu+j/2)}{(2+\eta^{-1}+\eta)^{\mu+j/2}\mu^{j/2}\Gamma(2\mu)}$$

$${}_{2}F_{1}\left[\mu + \frac{j}{4} + \frac{1}{2}, \mu + \frac{j}{4}; \mu + \frac{1}{2}; \left(\frac{1-\eta}{1+\eta}\right)^{2}\right]$$
(4)

where  $_2F_1\left(\cdot\right)$  is the Gauss hypergeometric function. Consequently, by utilizing equation (4), we can determine the mean and variance (at the top of the next page) as follows,

$$\varpi_m \triangleq E(P) = \frac{2^{(2\mu+1/2)}\Gamma(2\mu+1/2)}{(2+\eta^{-1}+\eta)^{\mu+1/2}\mu^{1/2}\Gamma(2\mu)} {}_{2}F_{1}\left[\mu + \frac{3}{4}, \mu + \frac{1}{4}; \mu + \frac{1}{2}; \left(\frac{1-\eta}{1+\eta}\right)^{2}\right] (5)$$

where  $\mathrm{E}\left(\cdot\right)$  and  $\mathrm{Var}\left(\cdot\right)$  are the expectation and variance operators respectively.

## III. OUTAGE PROBABILITY ANALYSIS

In this section, we derive the analytical expression for the OP within the proposed generalized framework. The statistical properties of  $\Upsilon$  are necessary to derive the analytical expression of the performance metric under consideration. With this, next we aim to find the mean and variance of  $\Upsilon$ . Recalling  $\delta_{kip}$  and  $\vartheta_{kiq}$  follow IID  $\eta{-}\mu$  distribution functions, we have the following,

$$E\left[\delta_{lin}\theta_{lia}\right] = E\left[\delta_{lin}\right]E\left[\theta_{lia}\right] = \varpi_m^2 \tag{7}$$

$$\varpi_v \triangleq \operatorname{Var}(P) = \left(\frac{4}{2+\eta^{-1}+\eta}\right)^{\mu+1} {}_{2}F_{1}\left[\mu+1, \mu+\frac{1}{2}; \mu+\frac{1}{2}; \left(\frac{1-\eta}{1+\eta}\right)^{2}\right] - \left[\frac{2^{(2\mu+1/2)}\Gamma(2\mu+1/2)}{(2+\eta^{-1}+\eta)^{\mu+1/2}\mu^{1/2}\Gamma(2\mu)} {}_{2}F_{1}\left[\mu+\frac{3}{4}, \mu+\frac{1}{4}; \mu+\frac{1}{2}; \left(\frac{1-\eta}{1+\eta}\right)^{2}\right]\right]^{2}$$
 (6)

$$\operatorname{Var}\left[\delta_{lip}\vartheta_{liq}\right] = \operatorname{Var}\left[\delta_{lip}\right] \operatorname{Var}\left[\vartheta_{liq}\right] + \operatorname{Var}\left[\delta_{lip}\right] \left(\operatorname{E}\left[\vartheta_{liq}\right]\right)^{2} + \operatorname{Var}\left[\vartheta_{liq}\right] \left(\operatorname{E}\left[\delta_{lip}\right]\right)^{2} = \varpi_{v}^{2} + 2\varpi_{v}\varpi_{m}^{2}$$
(8)

Consequently, the statistics of  $\Upsilon$  can be derived as,

$$\Lambda_e \triangleq \mathrm{E}[\Upsilon] = \mathrm{E}\left[\sum_{l=1}^{Z} \sum_{i=1}^{N_l} \sum_{p=1}^{L_t} \sum_{q=1}^{L_r} \delta_{lip} \vartheta_{liq}\right] = ZN_l L_t L_r \varpi_m^2$$

$$\Lambda_v^2 \triangleq \operatorname{Var}[\Upsilon] = \operatorname{Var}\left[\sum_{l=1}^Z \sum_{i=1}^{N_l} \sum_{p=1}^{L_t} \sum_{q=1}^{L_r} \delta_{lip} \vartheta_{liq}\right] 
= ZN_k L_t L_r \left(\varpi_v^2 + 2\varpi_v \varpi_m^2\right)$$
(10)

Recalling  $\gamma = \Upsilon^2 \zeta$  and  $\Upsilon^2$  is a NCCS distribution with one degree of freedom having parameters  $\Lambda_e$  and  $\Lambda_v^2$ , the PDF of  $\Upsilon^2$  can be given as [33],

$$f_{\Upsilon^2}(s) = \frac{1}{2\Lambda_v^2} \left(\frac{s}{\Lambda_e}\right)^{-\frac{1}{4}} e^{\frac{-(s+\Lambda_e)}{2\Lambda_v^2}} I_{-\frac{1}{2}} \left[\frac{\sqrt{s\Lambda_e}}{\Lambda_v^2}\right]$$
(11)

Accordingly, the PDF of  $\gamma$  can be written as,

$$f_{\gamma}\left(w\right) = \frac{1}{2\Lambda_{v}^{2}\zeta} \left(\frac{w}{\zeta\Lambda_{e}}\right)^{-\frac{1}{4}} e^{\frac{-(w+\zeta\Lambda_{e})}{2\zeta\Lambda_{v}^{2}}} I_{-\frac{1}{2}} \left[\frac{1}{\Lambda_{v}^{2}} \sqrt{\frac{w\Lambda_{e}}{\zeta}}\right]$$
(12)

In order to find out the dead zones caused by blockages, one has to find out the outage probability. To this end, the probability that the received SNR falls below a specified threshold value ( $\gamma_{th}$ ) at the Rx can be expressed as [26], [35],

$$P_{\text{outage}} = \Pr\left(\gamma < \gamma_{th}\right) = \int_{-\infty}^{\gamma_{th}} f_{\gamma}\left(w\right) dw$$
$$= 1 - \int_{\gamma_{th}}^{\infty} f_{\gamma}\left(w\right) dw \qquad (13)$$

$$\textstyle \int_{\gamma_{th}}^{\infty} f_{\gamma}\left(w\right) dw = \int_{w=\gamma_{th}}^{\infty} \frac{1}{2\Lambda_{v}^{2}\zeta} \left(\frac{w}{\zeta\Lambda_{e}}\right)^{-\frac{1}{4}} \mathrm{e}^{\frac{-\left(w+\zeta\Lambda_{e}\right)}{2\zeta\Lambda_{v}^{2}}} I_{-\frac{1}{2}} \left[\frac{1}{\Lambda_{v}^{2}}\sqrt{\frac{w\Lambda_{e}}{\zeta}}\right] dw$$

Substituting  $\frac{w}{\zeta \Lambda_v^2} = \tau^2$ , the above equation can be modified as

$$\int_{\gamma_{th}}^{\infty} f_{\gamma}(w) dw = \frac{1}{\left(\frac{\Lambda_{e}^{2}}{\Lambda_{v}}\right)^{-\frac{1}{2}}} \int_{\sqrt{\frac{\gamma_{th}}{\zeta \Lambda_{v}^{2}}}}^{\infty} \tau^{\frac{1}{2}} e^{-\left(\frac{\tau^{2} + \frac{\Lambda_{e}}{\Lambda_{v}^{2}}}{2}\right)} I_{m-1} \left[\sqrt{\frac{\Lambda_{e}}{\Lambda_{v}^{2}}} \tau\right] d\tau$$
(14)

The Marcum-Q function can be given as [35],

$$Q_m\left(a,b\right) = \frac{1}{a^{m-1}} \int_b^\infty \tau^m \mathrm{e}^{-\left(\frac{\tau^2 + a^2}{2}\right)} I_{m-1}\left(a\tau\right) d\tau \quad (15)$$

Now comparing equations (14) and (15), we have the following,

$$\int_{\gamma_{th}}^{\infty} f_{\gamma}(w) dw = Q_{\frac{1}{2}} \left( \sqrt{\frac{\Lambda_e}{\Lambda_v^2}}, \sqrt{\frac{\gamma_{th}}{\zeta \Lambda_v^2}} \right)$$
 (16)

TABLE III SIMULATION PARAMETERS [28], [37]

Description	Values
Number of reflecting elements, N	36 - 576
Distance between Tx to Rx, d	100 m
Height of IRS $(h_I)$	15 m
Height of Tx $(h_T)$	10 m
Height of Rx $(h_R)$	2 m
Path loss Exponent, $\alpha$	3
Outage threshold, $\gamma_{th}$	10 dB
Carrier frequency $(f_c)$	3 GHz
Transmit power $(P_x)$	[0, 30]  dBm
Power dissipated per IRS element $(P_i)$ [mW]	7.8
Power conversion efficiency $(\xi)$	80%
Circuit dissipated power at Tx $(P_c^{Tx})$ [dBm]	10
Circuit dissipated power at Rx $(P_c^{Rx})$ [dBm]	10
Hardware static power of phase shift circuit $(P_{ps})$ [dBm]	10
Bandwidth	10 MHz
Noise Figure	10 dBm
Modulation scheme	M-PSK

Finally, using equation (16) in equation (13), the outage probability of the considered system model can be derived as follows,

$$P_{\text{outage}} = 1 - Q_{\frac{1}{2}} \left( \sqrt{\frac{\Lambda_e}{\Lambda_v^2}}, \sqrt{\frac{\gamma_{th}}{\zeta \Lambda_v^2}} \right)$$
 (17)

where  $Q_{\frac{1}{2}}(A,B)$  is the fractional order 1/2 generalized Marcum Q-function and may be written in terms of Gaussian-Q function as [36],

$$Q_{\frac{1}{2}}(A,B) = Q(B-A) + Q(B+A)$$
 (18)

Consequently, the OP can be restructured as shown here,

$$P_{\text{outage}} = Q\left(\sqrt{\frac{\gamma_{th}}{\zeta\Lambda_v^2}} - \sqrt{\frac{\Lambda_e}{\Lambda_v^2}}\right) + Q\left(\sqrt{\frac{\gamma_{th}}{\zeta\Lambda_v^2}} + \sqrt{\frac{\Lambda_e}{\Lambda_v^2}}\right)$$
(19)

# IV. ENERGY EFFICIENCY

The EE of an IRS-assisted system can be described as [28],

$$EE = BW \times \left(\frac{R}{P_{total}}\right)$$
 (20)

where BW is the bandwidth of the system,  $R=b\times BW$  represents the rate at which bits are transmitted, where b signifies the bits per symbol (for BPSK, b=1).  $P_{\rm total}$  denotes the comprehensive power utilized by the system to attain a specified BER, which can be calculated as,

$$P_{\text{total}} = P_x + P_x^{HPA} + P_c^{Tx} + NP_i + NP_{ps} + P_c^{Rx}$$
 (21)

where  $P_x$  is power used for transmitting the information,  $P_x^{HPA} = \frac{P_x}{\xi}$  is the power consumed by the high power amplifier (HPA) with  $\xi$  being the power conversion efficiency (80%),  $P_i$  is power at the  $i^{th}$  IRS element,  $P_{ps}$  is the hardware static power of phase-shift circuit,  $P_c^{Tx}$  is circuit power at the transmitter and  $P_c^{Rx}$  is circuit power at the receiver.

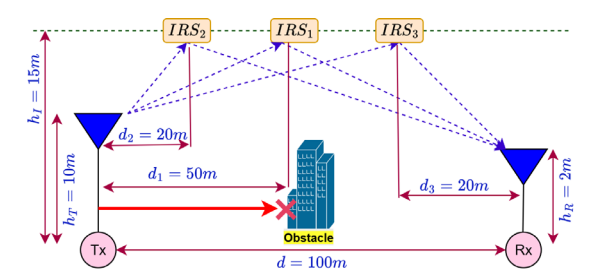


Fig. 2. MC simulation setup.

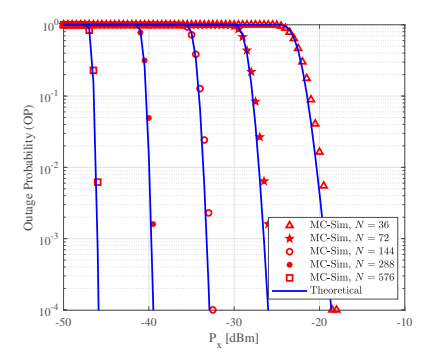


Fig. 3. Outage probability versus source transmit power  $(P_x)$  with  $\eta=1$ ,  $\mu=0.5,\ L_t=L_r=2$ , and S-IRS, varying N.

### V. RESULTS AND DISCUSSIONS

This section presents the outcomes of the derived OP for the system model under consideration for Single IRS (S-IRS), Double IRS (D-IRS), and Triple IRS (T-IRS). The simulation of MC is established based on the parameters outlined in Table III, aimed at both validating the accuracy of the derived analytical expressions and gaining further insights into the variables influencing overall system performance. The comparison among various IRSs is performed by maintaining an equal number of reflective elements used in S-IRS, D-IRS, and T-IRS systems, specifically  $N_1=2N_2=3N_3=N$ . The simulation configuration is established in accordance with Fig. 2.

# A. OP Results

Fig. 3 illustrates the impact of N on the OP. The strong agreement between the simulated and theoretical results once again confirms the accuracy of the obtained formulas in Section III and the OP decreases as N increases. This improved OP performance can be traded with the transmit power. For instance, if an OP of  $10^{-4}$  is deemed appropriate for a specific wireless system, subsequently utilizing N=576 will result in achieving this at approximately  $P_x=-46$  dBm, and with N=36, it can be achieved at  $P_x=-18.5$  dBm. Therefore, by increasing the number of reflecting elements, it is possible to achieve a gain of 27.5 dBm. Furthermore, as the value of  $P_x$  increases, the OP decreases significantly for a fixed N.

Fig. 4 shows the effect of  $\eta$ ,  $\mu$  on the OP performance. The accuracy of the derived expressions is once again confirmed. Based on Fig. 4, it can be deduced that the increases in the  $\eta$ ,  $\mu$  values lead to a decrease in the OP. For instance, when ensuring a constant OP  $10^{-2}$ , an increase in  $\mu$  from 0.5 to

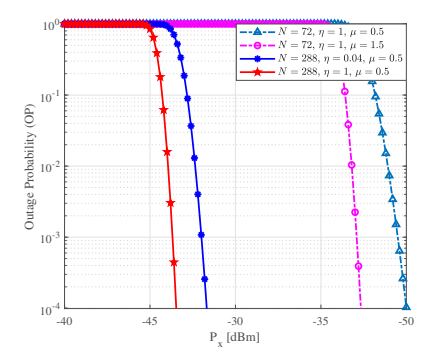


Fig. 4. Outage probability versus source transmit power  $(P_x)$  with  $N=72,288,\, L_t=L_r=2,$  and D-IRS, varying  $\eta,\,\mu$ 

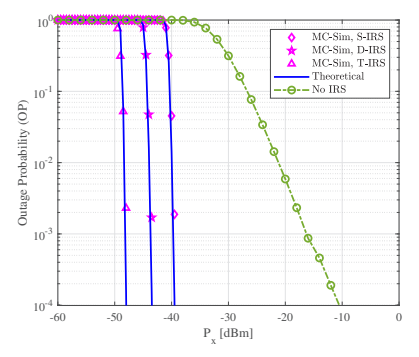


Fig. 5. Outage probability versus source transmit power  $(P_x)$  for S-IRS, D-IRS, T-IRS, and No IRS cases with  $N=288,~\eta=1,~\mu=0.5,$  and  $L_t=L_r=2.$ 

1.5 leads to a transmit power improvement of 2.1 dBm, and also, an increase in  $\eta$  from 0.04 to 1 leads to a transmit power improvement of 1.5 dBm.

Fig. 5, illustrates the OP performance for S-IRS, D-IRS, and T-IRS systems, along with a baseline comparison to a conventional MIMO system without IRS (denoted as "No IRS"). The graph demonstrates that the theoretical results derived in Section III are in close agreement with the outcomes obtained through MC simulations. It is evident that an increase in  $P_x$  leads to a significant reduction in OP. Furthermore, the OP decreases as the number of IRSs increases. One can note that an increase in  $P_x$  results in a noticeable decline in OP. In addition, as the number of IRSs increases the OP decreases. For example, consider an outage probability of  $10^{-4}$ , the transmit power  $P_x$  approximately -39 dBm, -43 dBm, and -46 dBm for S-IRS, D-IRS, and T-IRS, respectively. In contrast, the conventional "No IRS" system requires significantly higher transmit power approximately -10 dBm to achieve the same OP, clearly illustrating the efficiency and effectiveness of IRS-assisted communication. These results affirm that multi-IRS deployment not only improves reliability but also enables substantial transmit power savings compared to traditional non-IRS MIMO systems.

The influence of different values of  $L_t, L_r$  on the OP is depicted in Fig. 6. The OP results obtained from theoretical analysis for the multi-antenna systems for S-IRS are in complete agreement with the simulated results. Based on the information provided in Fig. 6, it is clear that the outage performance improves significantly as the number of transmitting

# Improved Outage Probability using Multi-IRS-Assisted MIMO Wireless Communications in Cellular Blockage Scenarios

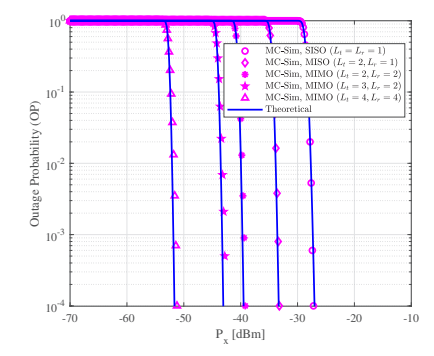


Fig. 6. Outage probability versus source transmit power ( $P_x$ ) with N=288,  $\eta=1,\,\mu=0.5,\,$  S-IRS, varying  $L_t,L_r.$ 

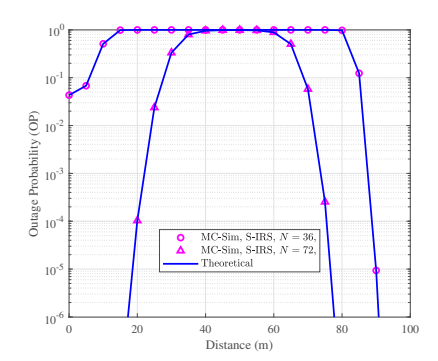


Fig. 7. Outage probability versus distance with N=36,72,  $\eta=1,$   $\mu=0.5,$  S-IRS,  $L_t=L_r=2,$   $P_x=30$  dBm.

and receiving antennas increases in the S-IRS scenario. For example, consider an outage probability of  $10^{-4}$ , the number of Tx and Rx antennas  $(L_t, L_r)$  values increases from (1,1) to (4,4), the equivalent  $P_x$  values changes from -27.2 dBm to -51.2 dBm.

The impact of the user location on the outage probability is depicted in Fig. 7. Firstly, at a fixed  $P_x$ , the outage probability is less when the IRS is placed closer to either Tx or Rx. Secondly, as the number of reflecting elements changes from 36 to 72, the outage values decrease drastically. For instance, with N=36, an OP value of 0.0681 is attained when IRS is positioned 5m away from Tx, and with N=72 an OP value of 0.0238 is attained when IRS is 25m away from Tx and also 0.000254 is attained when IRS is 25m away from Rx.

Fig. 8 shows the Outage probability versus Number of reflecting elements (N) with  $\eta=1$ ,  $\mu=0.5$ , S-IRS, varying  $P_x$  dBm. The influence of different values of  $P_x$  dBm on the outage probability is depicted in Fig. 8, it is clear that the outage performance improves significantly as the source transmit power  $P_x$  dBm increases. In addition, as the number of reflecting elements increases the OP decreases.

Fig. 9 compares the OP performance of Random phase shift (RPS), Optimum phase shift (OPS), and Discrete phase shift (DPS) techniques with different quantization levels. The OPS scheme achieves the best performance due to perfect phase alignment, resulting in the lowest OP across all transmit power levels  $P_x$ . In contrast, RPS yields the poorest performance due to random phase shifts, resulting in higher OP. The DPS schemes serve as a practical compromise between OPS and

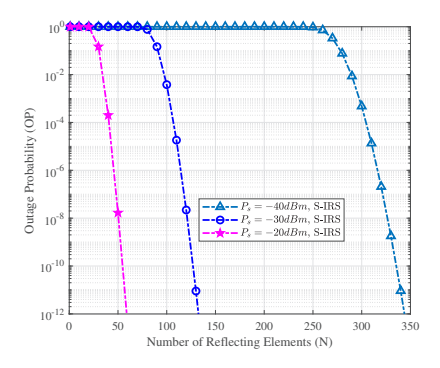


Fig. 8. Outage probability versus Number of reflecting elements (N) with  $\eta=1,~\mu=0.5,$  S-IRS, varying  $P_x$  dBm.

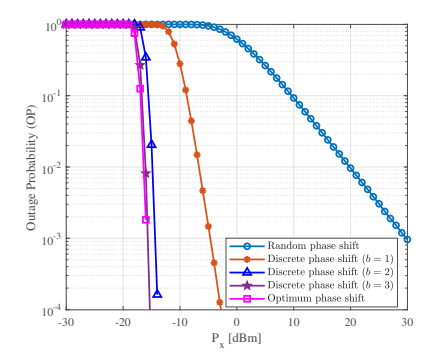


Fig. 9. Outage probability versus source transmit power  $(P_x)$  for multiple phases with  $L_t=L_r=1,~\eta=1,~\mu=1,~N=72,$  and S-IRS.

RPS. The performance of DPS improves as the number of quantization bits b increases, with 3-bit quantization (b=3) nearly matching the OPS curve. For instance, at an OP of  $10^{-3}$ , the required transmit powers are approximately 30 dBm, -5 dBm, -14 dBm, -16 dBm, and -16 dBm respectively for RPS, DPS (b=1), DPS (b=2), DPS (b=3), and OPS.

Fig. 10 shows the OP performance of a IRS-assisted communication system under  $\eta-\mu$  fading for various M-PSK modulation orders ( $M\in\{2,4,8,16\}$ ). As the modulation order increases, the system experiences higher OP at a given transmit power ( $P_x$ ). For example, to achieve an OP of  $10^{-3}$ , the required transmit power increases from approximately  $P_x=-14$  dBm, for M=2 to about  $P_x=-1$  dBm for M=16. This trend occurs because higher-order M-PSK schemes have denser constellations with reduced symbol

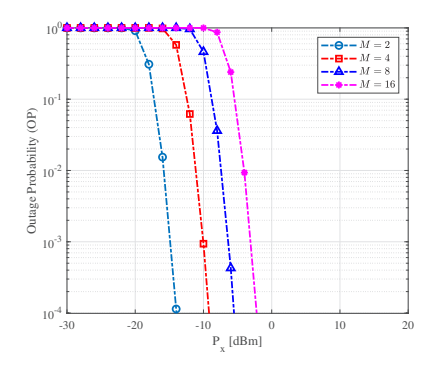


Fig. 10. Outage probability versus source transmit power  $(P_x)$  varying M (M-PSK) with  $L_t=L_r=2,~\eta=1,~\mu=1,~N=32,$  and S-IRS.

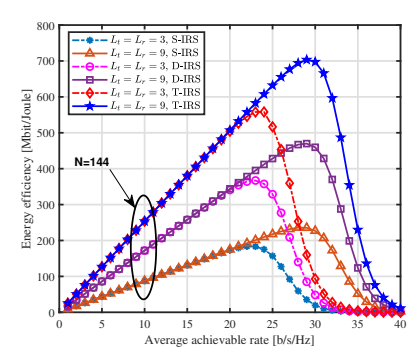


Fig. 11. Energy efficiency versus average achievable rate for varying  $L_t, L_r$  with fixed  $\eta=1,\,\mu=1,$  and N=144.

spacing, making them more susceptible to noise and channel fading. Therefore, more transmit power is required to maintain reliable communication as M increases.

In Fig. 11, we evaluate the EE of S-IRS, D-IRS, and T-IRS systems, all possessing an identical number of reflecting elements, while considering the total power consumption, which encompasses the circuit power dissipation of both the Tx, Rx, and the hardware impairments of IRS elements, in relation to the target spectral efficiency (R) with respect to equation (20). Firstly, the T-IRS system surpasses the D-IRS and S-IRS systems in terms of a fixed average achievable rate. For a rate of 30 b/s/Hz with  $(Z_t, Z_r) = (9, 9)$ , the EE (in Mbits/Joule) at S-IRS, D-IRS, and T-IRS are 226.94, 459.59, and 697.57, respectively. Furthermore, for elevated achievable rate values, the utilization of multiple IRSs proves more advantageous than the S-IRS system. Secondly, with a constant number of IRSs, an increase in the number of antennas at the BS enhances energy efficiency to attain the same achievable rate. The aforementioned observations are substantiated by the analysis presented in Section IV, which indicates that the T-IRS attains a superior rate relative to D-IRS and S-IRS, allowing for a trade-off between the target average achievable rate and energy efficiency as delineated in equation (20).

#### VI. CONCLUSIONS

This study examined the outage probability performance analysis of a multi-antenna MIMO communication system supported by multiple IRSs under a generalized  $\eta$ - $\mu$  fading environment. The proposed model targets NLOS scenarios, where direct Tx and Rx links are blocked, as commonly seen in urban environments. Using the central limit theorem, we derived the statistical properties of the received SNR for the system in terms of its first and second moments. Consequently, the theoretical expression for the OP utilizing the Q-function was obtained. Simulation results under various parameter configurations validate the accuracy of the theoretical analysis. Energy efficiency showed that the multi-IRS system outperformed the S-IRS system. The findings highlight that system performance is significantly affected by factors such as the number of IRSs, their placement, the count of reflecting elements, channel fading parameters, and the number of antennas at the Tx and Rx. Our findings show that incorporating multiple IRSs significantly improves link

reliability by lowering the OP in blockage-heavy areas. The performance benefits grow with more reflecting elements and higher values of  $\eta$  and  $\mu$  parameters. Additionally, the use of multiple antennas at both ends further enhances diversity gains. IRS placement also plays a vital role, with closer positioning to the Tx or Rx leading to noticeable improvements. Overall, the study demonstrates that a multi-antenna, multi-IRS MIMO system achieves better performance than a system supported by a single IRS and is also a promising solution for reliable and efficient next-generation wireless communication. The analysis may be expanded to encompass more generalized fading models, such as the  $\alpha$ - $\eta$ - $\mu$  distribution, to more accurately reflect real-world variability. Furthermore, integrating machine learning techniques for real-time IRS control can enhance adaptability and performance in dynamic wireless environments.

### REFERENCES

- [1] T. Padmavathil, K. K. Cheepurupalli, and R. Madhu, "Evaluation of fbmc channel estimation using multiple auxiliary symbols for high throughput and low ber 5g and beyond communications," *Infocommunications Journal*, vol. 16, no. 2, pp. 25–32, 2024, **DOI**: 10.36244/ICJ.2024.2.4.
- [2] R. Pestourie, C. Pérez-Arancibia, Z. Lin, W. Shin, F. Capasso, and S. G. Johnson, "Inverse design of large-area metasurfaces," *Optics express*, vol. 26, no. 26, pp. 33 732–33 747, 2018, DOI: 10.1364/OE.26.033732.
- [3] C. Huang, S. Hu, G. C. Alexandropoulos, A. Zappone, C. Yuen, R. Zhang, M. Di Renzo, and M. Debbah, "Holographic mimo surfaces for 6g wireless networks: Opportunities, challenges, and trends," *IEEE wireless communications*, vol. 27, no. 5, pp. 118–125, 2020, DOI: 10.1109/MWC.001.1900534.
- [4] Y. Liu, X. Liu, X. Mu, T. Hou, J. Xu, M. Di Renzo, and N. Al-Dhahir, "Reconfigurable intelligent surfaces: Principles and opportunities," *IEEE communications surveys & tutorials*, vol. 23, no. 3, pp. 1546– 1577, 2021, DOI: 10.1109/COMST.2021.3077737.
- [5] M. Chaudhary and S. K. Bandari, "A low complex joint optimization model for maximizing sum rate and energy efficiency in an irs-assisted multi-user communication scenario," *Physical Communication*, vol. 63, p. 102 296, 2024, **DOI**: 10.1016/j.phycom.2024.102296.
- [6] M. A. ElMossallamy, H. Zhang, L. Song, K. G. Seddik, Z. Han, and G. Y. Li, "Reconfigurable intelligent surfaces for wireless communications: Principles, challenges, and opportunities," *IEEE Transactions on Cognitive Communications and Networking*, vol. 6, no. 3, pp. 990–1002, 2020, **DOI**: 10.1109/TCCN.2020.2992604.
- [7] Z. Wang, L. Liu, S. Zhang, and S. Cui, "Massive mimo communication with intelligent reflecting surface," *IEEE Transactions on Wireless Communications*, vol. 22, no. 4, pp. 2566–2582, 2022, DOI: 10.1109/TWC.2022.3212537.
- [8] S. K. Bandari, V. Mani, and A. Drosopoulos, "Performance analysis of gfdm in various fading channels," COMPEL: The International Journal for Computation and Mathematics in Electrical and Electronic Engineering, vol. 35, no. 1, pp. 225–244, 2016, DOI: 10.1108/COMPEL-06-2015-0215.
- [9] S. K. Bandari, S. S. Yadav, and V. Mani, "Analysis of gfdm in generalized η-μ fading channel: A simple probability density function approach for beyond 5g wireless applications," AEU-International Journal of Electronics and Communications, vol. 153, p. 154 260, 2022, DOI: 10.1016/j.aeue.2022.154260.
- [10] R. Mallaiah and V. Mani, "A novel otfs system based on dfrft-ofdm," IEEE Wireless Communications Letters, vol. 11, no. 6, pp. 1156– 1160, 2022, DOI: 10.1109/LWC.2022.3159534.
- [11] W. Mei and R. Zhang, "Joint base station and irs deployment for enhancing network coverage: A graph-based modeling and optimization approach," *IEEE Transactions on Wireless Communications*, vol. 22, no. 11, pp. 8200–8213, 2023, DOI: 10.1109/TWC.2023.3260805.

# Improved Outage Probability using Multi-IRS-Assisted MIMO Wireless Communications in Cellular Blockage Scenarios

- [12] T. Hou, Y. Liu, Z. Song, X. Sun, Y. Chen, and L. Hanzo, "Reconfigurable intelligent surface aided noma networks," *IEEE Journal on Selected Areas in Communications*, vol. 38, no. 11, pp. 2575–2588, 2020, DOI: 10.1109/JSAC.2020.3007039.
- [13] L. Yang, W. Guo, and I. S. Ansari, "Mixed dual-hop fso-rf communication systems through reconfigurable intelligent surface," *IEEE Communications Letters*, vol. 24, no. 7, pp. 1558–1562, 2020, poi: 10.1109/LCOMM.2020.2986002.
- [14] S. Li, B. Duo, X. Yuan, Y.-C. Liang, and M. Di Renzo, "Reconfigurable intelligent surface assisted uav communication: Joint trajectory design and passive beamforming," *IEEE Wireless Communications Letters*, vol. 9, no. 5, pp. 716–720, 2020, poi: 10.1109/LWC.2020.2966705.
- [15] E. Björnson, Ö. Özdogan, and E. G. Larsson, "Intelligent reflecting surface versus decode-and-forward: How large surfaces are needed to beat relaying?" *IEEE Wireless Communications Letters*, vol. 9, no. 2, pp. 244–248, 2019, **DOI**: 10.1109/LWC.2019.2950624.
- [16] A. E. Canbilen, E. Basar, and S. S. Ikki, "Reconfigurable intelligent surface-assisted space shift keying," *IEEE wireless communications letters*, vol. 9, no. 9, pp. 1495–1499, 2020, DOI: 10.1109/LWC.2020.2994930.
- [17] W. Zhao, G. Wang, S. Atapattu, T. A. Tsiftsis, and C. Tellambura, "Is backscatter link stronger than direct link in reconfigurable intelligent surface-assisted system?" *IEEE Communications Letters*, vol. 24, no. 6, pp. 1342–1346, 2020, **DOI**: 10.1109/LCOMM.2020.2980510.
- [18] Q. Wu, G. Chen, Q. Peng, W. Chen, Y. Yuan, Z. Cheng, J. Dou, Z. Zhao, and P. Li, "Intelligent reflecting surfaces for wireless networks: Deployment architectures, key solutions, and field trials," *IEEE Wireless Communications*, 2025.
- [19] Y. Du, N. Qi, K. Wang, M. Xiao, and W. Wang, "Intelligent reflecting surface-assisted uav inspection system based on transfer learning," *IET Communications*, vol. 18, no. 3, pp. 214–224, 2024.
- [20] W. R. Braun and U. Dersch, "A physical mobile radio channel model," *IEEE transactions on Vehicular Technology*, vol. 40, no. 2, pp. 472–482, 1991, **DOI**: 10.1109/25.289429.
- [21] M. D. Yacoub, "The κ-μ distribution and the η-μ distribution," *IEEE Antennas and Propagation Magazine*, vol. 49, no. 1, pp. 68–81, 2007, poi: 10.1109/MAP.2007.370983.
- [22] M. H. Samuh, A. M. Salhab, and A. H. A. El-Malek, "Performance analysis and optimization of ris-assisted networks in nakagami-m environment," arXiv preprint arXiv:2010.07841, 2020.
- [23] M. A. A. Junior, G. Fraidenraich, R. C. Ferreira, F. A. De Figueiredo, and E. R. De Lima, "Multiple-antenna weibullfading wireless communications enhanced by reconfigurable intelligent surfaces," *IEEE Access*, vol. 11, pp. 107 218–107 236, 2023, por: 10.1109/ACCESS.2023.3310936.
- [24] R. M. Rafi and V. Sudha, "Ser and outage probability analysis of double ris assisted wireless communication system," Wireless Personal Communications, vol. 133, no. 4, pp. 2339–2354, 2023, DOI: 10.1007/s11277-024-10869-y.
- [25] R. K. Hindustani, S. Sharma, and D. Dixit, "Outage analysis of multi-irs wireless communication over κ-μ fading with panel selection," in 2024 5th International Conference on Innovative Trends in Information Technology (ICITIIT). IEEE, 2024, pp. 1–5, DOI: 10.1109/ICITIIT61487.2024.10580099.
- [26] L. Yang, Y. Yang, D. B. da Costa, and I. Trigui, "Outage probability and capacity scaling law of multiple ris-aided networks," *IEEE Wireless Communications Letters*, vol. 10, no. 2, pp. 256–260, 2020, DOI: 10.1109/LWC.2020.3026712.
- [27] Z. Zhang, Y. Cui, F. Yang, and L. Ding, "Analysis and optimization of outage probability in multi-intelligent reflecting surface-assisted systems," arXiv preprint arXiv:1909.02193, 2019, DOI: 10.48550/arXiv.1909.02193.
- [28] T. N. Do, G. Kaddoum, T. L. Nguyen, D. B. Da Costa, and Z. J. Haas, "Multi-ris-aided wireless systems: Statistical characterization and performance analysis," *IEEE Transactions on Communications*, vol. 69, no. 12, pp. 8641–8658, 2021, DOI: 10.1109/TCOMM.2021.3117599.
- [29] S. Penchala, M. Chaudhary, S. K. Bandari, and V. Mani, "Impact of nakagami-m fading channel on reconfigurable intelligent surface symbol error rate in non-line-of-sight scenarios," in 2022 IEEE 19th India Council International Conference (INDICON). IEEE, 2022, pp. 1–4, DOI: 10.1109/INDICON56171.2022.10040187.

- [30] P. Nayeri, F. Yang, and A. Z. Elsherbeni, *Reflectarray antennas:* theory, designs, and applications. John Wiley & Sons, 2018.
- [31] Q. Wu and R. Zhang, "Beamforming optimization for wireless network aided by intelligent reflecting surface with discrete phase shifts," *IEEE Transactions on Communications*, vol. 68, no. 3, pp. 1838–1851, 2019.
- [32] E. Basar, "Transmission through large intelligent surfaces: A new frontier in wireless communications," in 2019 European Conference on Networks and Communications (EuCNC). IEEE, 2019, pp. 112– 117, DOI: 10.1109/EuCNC.2019.8801961.
- [33] J. G. Proakis and M. Salehi, Digital communications. McGraw-hill, 2008.
- [34] M. D. Yacoub, "The  $\varkappa \mu$  distribution and the  $\eta \mu$  distribution," *IEEE Antennas and Propagation Magazine*, vol. 49, no. 1, pp. 68–81, 2007.
- [35] M. Simon, "Alouini. ms: Digital communication over fading channels," A John Wiley Sons.—2005.—900 p, 2005, DOI: 10.1109/TIT.2008.924676.
- [36] A. Annamalai, C. Tellambura, and J. Matyjas, "A new twist on the generalized marcum q-function qm(a, b) with fractional-order m and its applications," in 2009 6th IEEE Consumer Communications and Networking Conference, 2009, pp. 1–5, DOI: 10.1109/CCNC.2009.4784840.
- [37] M. H. N. Shaikh, V. A. Bohara, A. Srivastava, and G. Ghatak, "Performance analysis of intelligent reflecting surface-assisted wireless system with non-ideal transceiver," *IEEE Open Journal of the Communications Society*, vol. 2, pp. 671–686, 2021, DOI: 10.1109/OJ-COMS.2021.3068866.



Suresh Penchala received his B.Tech and M.Tech degrees in Electronics and Communication Engineering from JNTU Hyderabad, Telangana, India, in 2005 and 2008 respectively. He is currently pursuing a Ph.D. degree at the National Institute of Technology, Meghalaya, India. His research interests include intelligent Reflecting Surfaces, wireless communication beyond 5G, and signal processing for communication. He is an associate member of the Institute of Electronics and Telecommunication Engineers (IETE), India.



Shravan Kumar Bandari received his Ph.D. degree from, NIT Warangal, India in 2018. Received postdoctoral fellowship from GIGA Korea project at Seoul National University, South Korea, 2018-2019. Received ERASMUS-MUNDUS Euphrates scholarship from the European Union under the doctoral mobility programme at TEI of Patras, Greece (now changed to University of the Peloponnese), 2014-2015. Selected candidate to receive Erasmus-Mundus INTERWEAVE scholarship holder at Tallinn

University of Technology, Estonia, 2014-2015. He is twice scholarship holder from MHRD India. Since 2019, he has been with the National Institute of Technology Meghalaya, India as an Assistant Professor of Electronics and Communication Engineering. His research interest includes future wireless systems, multi-carrier waveforms for next-generation wireless systems, multi-antenna/multi-user channels, compressed sensing, and cognitive radio.



Venkata Mani Vakamulla received the B.E. and M.E. degrees in electronics and communication engineering from the College of Engineering, Andhra University, India, in 1992 and 2003, respectively, and the Ph.D. degree in electrical engineering from the Indian Institute of Technology Delhi, India, in 2009. She joined the Electronics and Communication Engineering Department, at NIT Warangal, in April 2008, as an Assistant Professor, where she has been a Professor, since July 2022. She has numerous

publications in credit in national and international conferences and journals. Her research interests include wireless communication and signal processing for communication. She is a fellow of the Institute of Electronics and Telecommunication Engineers (IETE), India.